Concurrent, Scheduled, or Hybrid Transmission Protocol for ISAC

Diluka Galappaththige*, Mohammadali Mohammadi†, and Chintha Tellambura*
*Department of Electrical and Computer Engineering, University of Alberta, Edmonton, AB, T6G 1H9, Canada.
†Centre for Wireless Innovation (CWI), Queen's University Belfast, BT3 9DT Belfast, U.K.
Email: diluka.lg@ualberta.ca, m.mohammadi@qub.ac.uk, ct4@ualberta.ca

***Abstract*—Integrated sensing and communication (ISAC) systems enable communication and sensing functions via three protocols, including (TP_1) concurrently using the same time-frequency resources, (TP_2) scheduling them independently, or (TP_3) a hybrid technique that combines both. Nevertheless, all existing studies rely on the first approach, and none provide a comprehensive performance evaluation of all three protocols. Thus, this paper offers an extensive performance evaluation of these protocols, emphasizing their advantages, limitations, and trade-offs. Specifically, we maximize the sum communication and/or sensing rate for all protocols in a full-duplex ISAC system with multiple users and targets. Numerical results reveal that protocols (TP_1) and (TP_3) necessitate a sensing metric considering both transmit and receiver beams to ensure adequate sensing performance. In contrast, although protocol (TP_2) can utilize more straightforward sensing metrics and avoid communication-sensing interference, it may not achieve high communication performance.**

I. Introduction

Emerging applications, such as autonomous vehicles operating in dynamic environments with numerous obstacles, require highly accurate environmental sensing for real-time navigation and traffic congestion avoidance [1], [2]. For instance, such vehicles typically need distance accuracy of $0.1\,\mathrm{m}$ to $0.5\,\mathrm{m}$, angle precision of 0.1° to 1°, and latencies of $1\,\mathrm{ms}$ to $10\,\mathrm{ms}$. However, the standard integrated sensing and communication (ISAC) protocol, referred to as TP_1, may fall short in achieving the required sensing accuracy due to significant communication interference on the sensing system [1]. We propose two transmission protocols, TP_2 and TP_3, to enable efficient C&S in ISAC systems for high-accuracy applications.

A. Motivation and Our Contributions

In ISAC, C&S can share the same hardware through different transmission protocols. These protocols include *i)* TP_1: performing both functions concurrently using the same time-frequency resources, *ii)* TP_2: scheduling them in different time-frequency resources, *iii)* TP_3: using a mixed (or hybrid) strategy that combines both methods (Fig. 1). Although there are many works on ISAC in the literature, almost all focus on TP_1 as the primary transmission protocol [3]–[5]. However, for applications demanding high sensing performance, TP_1 may not be sufficient due to the intensive communication interference on singing. Conversely, none of the existing literature provides a comprehensive comparison of the performance across these three protocols. This leaves a considerable gap in the literature, particularly in how they balance the trade-offs between C&S tasks in various settings. To this end, a comprehensive evaluation of these three protocols is required to establish the most suitable approach for different ISAC applications with varying C&S needs. This forms the main motivation for this work.

We investigate the performance of a full-duplex (FD) multi-user, multi-target ISAC system with TP_1, TP_2, and TP_3 protocols (Fig. 2). In this system model, the FD base station (BS) transmits downlink (DL) signals to convey information to multiple DL users and/or perform sensing tasks to detect multiple targets. The main contributions are as follows:

- Three transmission protocols are introduced for ISAC networks, specifically within a multi-user, multi-target FD ISAC system. This work is the first to outline these protocols in detail and offer a comprehensive performance evaluation that highlights their respective advantages and disadvantages.
- A sum communication and/or sensing rate maximization problem, ($(\mathcal{P}1)$ (10a)), is formulated for all protocols. Because this optimization problem is non-convex and NP-hard, an alternative optimization (AO) based algorithm is developed, incorporating manifold optimization (MO) and the generalized Rayleigh quotient approach. This solution leverages the geometric properties of manifold space to address the non-convexity of the problem.
- Numerical results show that with TP_1 and TP_3 protocols, it is essential to employ a sensing metric that considers both transmit and receiver beam gains, as standard metrics like transmit beampattern gain or mean squared error (MSE) may be inadequate. In contrast, while TP_2 can use more straightforward sensing metrics, such as transmit beampattern gain, and avoid interference between C&S due to scheduled transmissions, it is not ideal for applications that require high communication performance.

B. Previous Contributions

While FD ISAC has been extensively investigated [3]–[5], protocol TP_1 is the exclusive focus. No previous work has quantified TP_2 and TP_3 protocols. In particular, Xia *et al.* [3] proposed an FD waveform design for mono-static ISAC systems, where the classic pulsed radar waveform is flexibly time-multiplexed with radar-communication signals. The proposed waveform can improve the communication rate and enhance the probability of target detection, provided that self-interference (SI) is effectively suppressed. Liu *et al.* [4] developed an optimization framework to jointly design transmit and receive beamformers in a mono-static ISAC transceiver, considering a scenario with a single uplink (UL) user, a single DL user, and a single target. It aims to simultaneously maximize the UL and DL

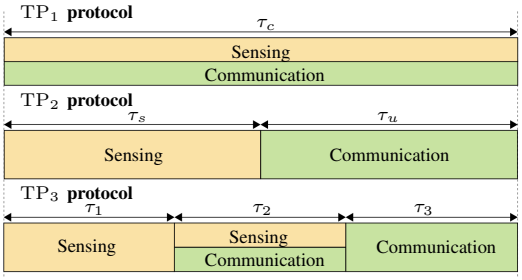

Fig. 1: Coherence time of transmission protocols.

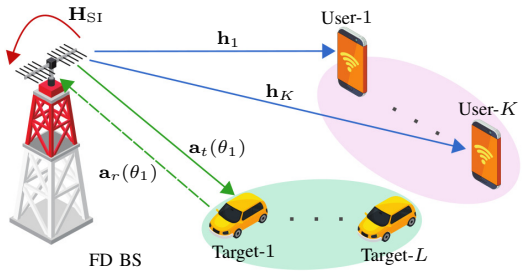

Fig. 2: An illustration of a general ISAC system setup.

rates, enhance the transmit and receive radar beampattern power at the target, and suppress residual SI. He *et al.* [5] extended the work in [4] to a multi-user scenario and jointly optimized the DL dual-functional transmit signal and the UL receive beamformers at the BS.

Notation: $\mathbf{I}_M$ and $\mathbf{0}_M$ are the $M \times M$ identity matrix and $M \times 1$ all-zero vector. $\Re(\cdot)$ denotes the real part. $\mathcal{CN}(\boldsymbol{\mu}, \mathbf{R})$ is a complex Gaussian vector with mean $\boldsymbol{\mu}$ and co-variance matrix $\mathbf{R}$. $\text{unt}(\mathbf{a}) = [a_1/|a_1|, \ldots, a_n/|a_n|]$.

II. Preliminaries

A. System and Channel Models

We consider an ISAC system consisting of an FD BS with M-transmit and N-receiver antenna arrays, K single-antenna communication users (i.e., U_k denotes the k-th user for $k \in \{1, \ldots, K\}$), and L potential targets (i.e., T_l denotes the l-th target for $l \in \{1, \ldots, L\}$) as shown in Fig. 2. BS antenna arrays are assumed to be uniform linear arrays (ULAs) with half-wavelength antenna spacing [5]. The BS uses the transmit signal to communicate with users in the DL and to perform radar sensing toward the potential target directions [5].

The BS captures the target-reflected signals and uses them to extract the targets' state information. To reduce SI, the BS uses two separate antenna sets for transmission and reception [5]. Time synchronization of the nodes is assumed for simplicity.

We consider block flat-fading channel models. During each fading block, $\mathbf{h}_k \in \mathbb{C}^{M\times 1}$ for $k \in \{1, \ldots, K\}$ is the the channel between the BS and U_k. These pure communication channels are modeled as Rayleigh fading and given as $\mathbf{h}_k = \zeta_k^{1/2}\tilde{\mathbf{h}}_k$, where ζ_k accounts for the large-scale path-loss and shadowing, which stays constant for several coherence intervals, and $\tilde{\mathbf{h}}_k \sim \mathcal{CN}(\mathbf{0}, \mathbf{I}_M)$ is the small-scale Rayleigh fading.

In contrast, adopting the echo signal representation in multiple-input and multiple-output (MIMO) radar systems, the channels between the BS transmit ULA and T_l and between the T_l and BS receiver ULA, i.e., $\mathbf{a}_t(\theta_l)$ and $\mathbf{a}_r(\theta_l)$, respectively, are modeled as line-of-sight (LoS) channels [5]. The transmit/receiver array steering vectors to the direction θ are thus given by $\mathbf{b}(\theta) = \frac{1}{\sqrt{B}}\left[1, e^{j\pi\sin(\theta)}, \ldots, e^{j\pi(B-1)\sin(\theta)}\right]^{\text{T}}$, where $\mathbf{b}(\cdot) \in \{\mathbf{a}_t(\cdot), \mathbf{a}_r(\cdot)\}$ and $B \in \{M, N\}$. It is assumed that T_l is located at angle θ_l. Finally, $\mathbf{H}_{\text{SI}} \in \mathbb{C}^{M\times N}$ is the SI channel matrix between the transmitter and the receiver ULAs of the BS. It is modeled as a Rician fading channel with a Rician factor of K_{SI} [6].

B. Transmission Protocols

The three C&S transmission protocols are shown in Fig. 1.

1) TP_1 *Protocol:* C&S occur concurrently during the coherence interval, τ, utilizing the entire interval. However, as C&S tasks take place simultaneously, they interfere mutually.

2) TP_2 *Protocol:* C&S are scheduled in two separate time slots, τ_s and τ_u, respectively, avoiding interference between the two operations. However, this limits the coherence time available for each function.

3) TP_3 *Protocol:* This is a hybrid protocol that combines TP_1 and TP_2. Thus, two independent sensing and communication phases, τ_1 and τ_3, respectively, and a concurrent C&S phase, τ_2, are allocated within the coherence interval.

Note that our primary goal is to compare the performance of these three protocols to determine the most effective transmission protocol for performing C&S in future ISAC networks.

C. Signal Model

The BS transmitted signal $\mathbf{x} \in \mathbb{C}^{M\times 1}$ can be expressed as

$$\mathbf{x} = \alpha_c \sum\nolimits_{i=1}^{K} \mathbf{w}_i q_i + \alpha_s \mathbf{s}, \tag{1}$$

where $q_i \in \mathbb{C}$ is the intended data symbol for U_i with unit power, i.e., $\mathbb{E}\{|q_i|^2\} = 1$, and $\mathbf{w}_i \in \mathbb{C}^{M\times 1}$ is the BS transmit beamforming vector for U_i, and $\mathbf{s} \in \mathbb{C}^{M\times 1}$ is the dedicated sensing signal at the BS [5]. It is also assumed that q_i and $\mathbf{s}$ are independent of each other [5]. In (1), $\alpha_c \in \{0, 1\}$ and $\alpha_s \in \{0, 1\}$ are the binary variables for enabling communication, sensing, or both based on the transmission protocol, i.e.,

$$\{\alpha_c, \alpha_s\} \triangleq \begin{cases} \text{TP}_1: & \{1,1\}, & \text{(2a)} \\ \text{TP}_2: & \begin{cases} \{0,1\}, & \text{for} \quad \tau_s, \\ \{1,0\}, & \text{for} \quad \tau_u, \end{cases} & \text{(2b)} \\ \text{TP}_3: & \begin{cases} \{0,1\}, & \text{for} \quad \tau_1, \\ \{1,1\}, & \text{for} \quad \tau_2, \\ \{1,0\}, & \text{for} \quad \tau_3. \end{cases} & \text{(2c)} \end{cases}$$

The received signal at U_k for $k \in \{1, \ldots, K\}$ is given by

$$y_k = \mathbf{h}_k^{\text{H}}\mathbf{x} + z_k = \alpha_c \sum\nolimits_{i=1}^{K} \mathbf{h}_k^{\text{H}}\mathbf{w}_i q_i + \alpha_s \mathbf{h}_k^{\text{H}}\mathbf{s} + z_k, \tag{3}$$

where $z_k \sim \mathcal{CN}(0, \sigma^2)$ denotes the additive white Gaussian noise (AWGN) at U_k.

The BS processes the target echo, i.e., reflected signal from the target, to extract the target's state information [5]. The received signal at the BS, i.e., $\mathbf{y}_b \in \mathbb{C}^{N\times 1}$, is expressed as

$$\mathbf{y}_b = \sum\nolimits_{j=1}^{L} \beta_j \mathbf{A}(\theta_j)\mathbf{x} + \sqrt{\beta_{\text{SI}}}\mathbf{H}_{\text{SI}}^{\text{H}}\mathbf{x} + \mathbf{z}_b, \tag{4}$$

where $\mathbf{A}(\theta_j) \triangleq \mathbf{a}_r(\theta_j)\mathbf{a}_t^{\mathrm{H}}(\theta_j)$ and $\mathbf{z}_b \sim \mathcal{CN}(\mathbf{0}, \sigma^2\mathbf{I}_N)$ is the BS AWGN vector. In (4), $\beta_j\mathbf{A}(\theta_j)\mathbf{x}$ is T_j's reflection, where $\beta_j \in \mathbb{C}$ is the complex amplitude of T_j reflection, accounting for the round-trip path-loss and the radar cross-section (RCS) of the target [7]. In particular, path loss accounts for signal attenuation over distance, whereas RCS determines how much power is reflected toward the BS based on the target's size, shape, and materials. It is also assumed that BS uses clutter rejection techniques to minimize the reflected clutter interference from the surrounding environment [8]. The second term in (4) represents the SI at the BS receiver, resulting from simultaneous FD transmission and reception, and $0 < \beta_{\mathrm{SI}} \ll 1$ is a constant that quantifies the SI cancellation ability of the FD BS [6]. We assume imperfect SI cancellation at the BS. The BS applies the sensing combiner, $\mathbf{u}_l \in \mathbb{C}^{N\times 1}$, to capture the desired reflected signal of T_l. The post-processed signal to extract the T_l's state information is given by

$$y_{b,l} = \beta_l \mathbf{u}_l^{\mathrm{H}}\mathbf{A}(\theta_l)\mathbf{x} + \sum\nolimits_{j\neq l}^{L} \beta_j \mathbf{u}_l^{\mathrm{H}}\mathbf{A}(\theta_j)\mathbf{x} + \sqrt{\beta_{\mathrm{SI}}}\mathbf{u}_l^{\mathrm{H}}\mathbf{H}_{\mathrm{SI}}\mathbf{x} + \mathbf{u}_l^{\mathrm{H}}\mathbf{z}_b. \quad (5)$$

Before proceeding to analyze C&S performance, it is necessary to clarify the assumptions: (i) the angles of a target at the BS transmitter and receiver ULAs are identical for co-located antenna arrays [8], (ii) θ_l and β_l are assumed to be pre-estimated or known at the BS for beamforming/combiner design [5], and (iii) before FD transmission, a separate channel estimation phase is employed to ensure that channel state information is available for beamforming design and SI cancellation at the BS.

III. Communication and Sensing Performance

System performance is determined by the communication rates of the users and the targets' detection rate in the BS.

Several mathematical notations are now defined for convenience. First, the BS beamforming vectors are encapsulated into a single matrix $\mathbf{W} = [\mathbf{w}_1, \ldots, \mathbf{w}_K, \mathbf{s}] \in \mathbb{C}^{M\times(K+1)}$. Next, to effectively manage C&S beamforming selections, a selection matrix is introduced as $\mathbf{E} = \mathbf{I}_{K+1}$. The combination of $\mathbf{W}$ and $\mathbf{E}$ allows for individual representation of each column from $\mathbf{W}$.

A. Communication Performance

The users utilize the received signal from the BS to decode their intended information. From (3), under TP_n protocol (for $n \in \{1,2,3\}$), the received signal-to-interference-plus-noise ratio (SINR) at U_k can be obtained as

$$\gamma_k^{\mathrm{TP}_n} = \frac{\alpha_c^2|\mathbf{h}_k^{\mathrm{H}}\mathbf{W}\mathbf{E}_k|^2}{\alpha_c^2\sum_{i\neq k}^{K}|\mathbf{h}_k^{\mathrm{H}}\mathbf{W}\mathbf{E}_i|^2 + \alpha_s^2|\mathbf{h}_k^{\mathrm{H}}\mathbf{W}\mathbf{E}_{K+1}|^2 + \sigma^2}, \quad (6)$$

where $\mathbf{E}_i$ is the i-th column of $\mathbf{E}$. Thus, the rate of U_k for all three transmission protocols can be approximated by

$$\mathcal{R}_k^{\mathrm{com}} = \begin{cases} \log_2(1+\gamma_k^{\mathrm{TP}_1}), & \mathrm{TP}_1, \\ \frac{\tau_u}{\tau_c}\log_2(1+\gamma_k^{\mathrm{TP}_2}), & \mathrm{TP}_2, \\ \frac{\tau_2}{\tau_c}\log_2(1+\gamma_k^{\mathrm{TP}_3}) + \frac{\tau_3}{\tau_c}\log_2(1+\gamma_k^{\mathrm{TP}_3}), & \mathrm{TP}_3. \end{cases} \quad (7)$$

Note that the SINR term in $\mathcal{R}_k^{\mathrm{com}}$ varies based on the transmission protocol and phase. Specifically, in TP_3, α_c and α_s take distinct values during phases τ_2 and τ_3, differentiating the SINR term in these two phases.

B. Sensing Performance

Sensing performance is typically evaluated by the transmit beampattern gain or MSE of the transmit beampattern [9]. While simple, they do not account for the receiver's beam pattern. As a remedy, the sensing SINR or rate has been suggested to assess sensing performance [5], [10]. The detection probability of a target is proportional to its sensing SINR [5], [10]. Conversely, the sensing SINR enables target detection through both transmit and receiver beamforming. Due to these benefits, we utilize sensing SINR (sensing rate) to measure sensing performance. By invoking (5), the sensing SINR of T_l at the BS under the TP_n protocol is given as

$$\Upsilon_l^{\mathrm{TP}_n} = \frac{|\beta_l|^2\mathbb{E}\left\{|\mathbf{u}_l^{\mathrm{H}}\mathbf{A}(\theta_l)\mathbf{x}|^2\right\}}{\sum_{j\neq l}^{L}|\beta_j|^2\mathbb{E}\left\{|\mathbf{u}_l^{\mathrm{H}}\mathbf{A}(\theta_j)\mathbf{x}|^2\right\} + \beta_{\mathrm{SI}}\mathbb{E}\left\{|\mathbf{u}_l^{\mathrm{H}}\mathbf{H}_{\mathrm{SI}}\mathbf{x}|^2\right\} + \mathbb{E}\left\{|\mathbf{u}_l^{\mathrm{H}}\mathbf{z}_b|^2\right\}} = \frac{|\beta_l|^2\mathbf{u}_l^{\mathrm{H}}\mathbf{A}(\theta_l)\mathbf{R}_x\mathbf{A}(\theta_l)^{\mathrm{H}}\mathbf{u}_l}{\mathbf{u}_l^{\mathrm{H}}\mathbf{Q}_l\mathbf{u}_l}, \quad (8)$$

where $\mathbf{Q}_l = \sum_{j\neq l}^{L}|\beta_j|^2\mathbf{A}(\theta_j)\mathbf{R}_x\mathbf{A}(\theta_j)^{\mathrm{H}} + \beta_{\mathrm{SI}}\mathbf{H}_{\mathrm{SI}}\mathbf{R}_x\mathbf{H}_{\mathrm{SI}}^{\mathrm{H}} + \sigma^2\mathbf{I}_N$, with $\mathbf{R}_x \triangleq \mathbb{E}\{\mathbf{x}\mathbf{x}^{\mathrm{H}}\} = \alpha_c^2\sum_{i=1}^{K}\mathbf{W}\mathbf{E}_i(\mathbf{W}\mathbf{E}_i)^{\mathrm{H}} + \alpha_s^2\mathbf{W}\mathbf{E}_{K+1}(\mathbf{W}\mathbf{E}_{K+1})^{\mathrm{H}}$ is the covariance matrix of the BS transmitted signal in (1). Thus, the sensing rate of T_l for all transmission protocols can be approximated as

$$\mathcal{R}_l^{\mathrm{Sen}} \approx \begin{cases} \log_2(1+\Upsilon_l^{\mathrm{TP}_1}), & \mathrm{TP}_1, \\ \frac{\tau_s}{\tau_c}\log_2(1+\Upsilon_l^{\mathrm{TP}_2}), & \mathrm{TP}_2, \\ \frac{\tau_1}{\tau_c}\log_2(1+\Upsilon_l^{\mathrm{TP}_3}) + \frac{\tau_2}{\tau_c}\log_2(1+\Upsilon_l^{\mathrm{TP}_3}), & \mathrm{TP}_3. \end{cases} \quad (9)$$

IV. Problem Formulation

For all three protocols, our objective is to maximize the C&S sum rate by optimizing the BS communication beamforming, $\{\mathbf{w}_i\}_{i=1}^K$, sensing signal, $\mathbf{s}$, and sensing combiners, $\{\mathbf{u}_l\}_{l=1}^L$, while adhering to the maximum BS transmit power constraint. The optimization problem is formulated as

$$(\mathcal{P}1): \max_{\mathbf{W},\{\mathbf{u}_l\}} \quad \sum\nolimits_{k=1}^{K}\mathcal{R}_k^{\mathrm{Com}} + \sum\nolimits_{l=1}^{L}\mathcal{R}_l^{\mathrm{Sen}}, \quad (10a)$$

$$\text{s.t.} \quad \mathrm{Tr}(\mathbf{W}\mathbf{W}^{\mathrm{H}}) \leq p_{\max}, \quad (10b)$$

$$\|\mathbf{u}_l\|^2 = 1, \quad \forall l, \quad (10c)$$

where (10b) sets the maximum BS transmit power constraint, with a maximum allowable transmit power of $p_{\max}$, and (10c) is the normalization constraint for the BS sensing combiner.

V. Proposed Solution

The problem $(\mathcal{P}1)$ is non-convex due to the involved product of optimization variables in the objective function. To handle it, the AO strategy is employed, decomposing $(\mathcal{P}1)$ into two sub-problems and solving one at a time while keeping the other fixed [11]. The process repeats until a stopping condition is reached. This method works when directly optimizing all variables is difficult or computationally expensive [11].

Note that for the sake of brevity, we only provide the solution for the TP_1 protocol, i.e., $\alpha_c = \alpha_s = 1$, which incorporates concurrent C&S, making it more challenging. However, the approach is easily adaptable to the other two protocols.

A. Sub-Problem 1: Optimizing $\{\mathbf{u}_l\}$

For fixed $\mathbf{W}$, the sensing rate $\mathcal{R}_l^{\mathrm{Sen}}$ is the only term that depends on $\{\mathbf{u}_l\}$. Since $\mathcal{R}_l^{\mathrm{Sen}}$ is a monotonically increasing function of its argument, i.e., Υ_l, we replace $\mathcal{R}_l^{\mathrm{Sen}}$ with Υ_l. Thus, using (8), we have the following optimization problem:

$$(\mathcal{P}2): \max_{\{\mathbf{u}_l\}} \quad \frac{\mathbf{u}_l^{\mathrm{H}}\mathbf{f}_l\mathbf{f}_l^{\mathrm{H}}\mathbf{u}_l}{\mathbf{u}_l^{\mathrm{H}}\mathbf{Q}_l\mathbf{u}_l}, \quad \text{s.t} \quad (10c), \tag{11a}$$

where $\mathbf{f}_l = \beta_l \mathbf{A}(\theta_l)\left(\sum_{i=1}^{K+1}\mathbf{W}\mathbf{E}_i\right)$. Problem $(\mathcal{P}2)$ resembles a generalized Rayleigh ratio quotient problem [12]. The optimal sensing combiner is thus given by

$$\mathbf{u}_l^* = \mathbf{Q}_l^{-1}\mathbf{f}_l / \|\mathbf{Q}_l^{-1}\mathbf{f}_l\|, \quad \forall l, \tag{12}$$

which is a minimal mean-squared error (MMSE) filter [12].

B. Sub-Problem 2: Optimizing $\mathbf{W}$

For given $\{\mathbf{u}_l\}$, the problem $(\mathcal{P}1)$ reduces to the following equivalent problem:

$$(\mathcal{P}3): \max_{\mathbf{W}} \quad \sum\nolimits_{k=1}^{K}\log_2(1+\gamma_k)+\sum\nolimits_{l=1}^{L}\log_2(1+\Upsilon_l), \tag{13a}$$

$$\text{s.t.} \quad (10b). \tag{13b}$$

This non-convex problem $(\mathcal{P}3)$ is addressed by using MO and fractional programming (FP). First, we introduce auxiliary variables $\boldsymbol{\mu} = [\mu_1, \ldots, \mu_{K+L}]$, such that $\mu_k \le \gamma_k$ for $k \in \{1, \ldots, K\}$ and $\mu_{K+l} \le \Upsilon_l$ for $l \in \{1, \ldots, L\}$, for each SINR term to handle the challenges imposed by the sum-log terms in the objective function (13). Then, $(\mathcal{P}3)$ is equivalently reformulated as [13]

$$(\mathcal{P}4): \max_{\mathbf{W},\boldsymbol{\mu}} \quad f(\mathbf{W},\boldsymbol{\mu}) = \frac{1}{\ln(2)}\sum\nolimits_{i=1}^{K+L}\ln(1+\mu_i) + \frac{1}{\ln(2)}\sum\nolimits_{i=1}^{K+L}\left(-\mu_i + \frac{(1+\mu_i)\bar{\gamma}_i}{1+\bar{\gamma}_i}\right), \tag{14a}$$

$$\text{s.t.} \quad (10b), \tag{14b}$$

where $\bar{\gamma}_i = \gamma_i$ for $i \in \{1, \ldots, K\}$ and $\bar{\gamma}_i = \Upsilon_i$ for $i \in \{K+1, \ldots, K+L\}$. $(\mathcal{P}4)$ can be divided into two parts: (i) an outer optimization over $\mathbf{W}$ with fixed $\boldsymbol{\mu}$ and (ii) an inner optimization over $\boldsymbol{\mu}$ with fixed $\mathbf{W}$ [13]. To solve $(\mathcal{P}4)$, $\mathbf{W}$ and $\boldsymbol{\mu}$ are alternately optimized until the objective function converges.

1) Optimizing $\boldsymbol{\mu}$: For a fixed $\mathbf{W}$, $f(\mathbf{W},\boldsymbol{\mu})$ is concave and differentiable with respect to $\boldsymbol{\mu}$. Therefore, the optimal $\boldsymbol{\mu}$ is obtained by setting each $\frac{\partial f(\mathbf{W},\boldsymbol{\mu})}{\partial \mu_k}$ equal to zero. The optimal μ_k is given by $\mu_k^* = \bar{\gamma}_k$ for $k \in \{1, \ldots, K\}$. Substituting $\boldsymbol{\mu}^*$ back into $f(\mathbf{W},\boldsymbol{\mu})$ recovers the exact sum-of-logarithms objective function in $(\mathcal{P}3)$.

2) Optimizing $\mathbf{W}$: For a fixed $\boldsymbol{\mu}$, we simplify the objective (14) by eliminating the constant terms with respect to $\mathbf{W}$. As a result, $(\mathcal{P}4)$ is reformulated as follows:

$$(\mathcal{P}5): \max_{\mathbf{W}} \quad f(\mathbf{W}), \quad \text{s.t.} \quad (10b), \tag{15a}$$

where $\hat{\mu}_k = 1 + \mu_k$ for $k \in \{1, \ldots, K+L\}$ and $f(\mathbf{W})$ is given in (16) with $\mathbf{g}_{lj} \triangleq \mathbf{u}_l^{\mathrm{H}}\mathbf{A}(\theta_j)$ and $\mathbf{g}_{\mathrm{SI},l} \triangleq \mathbf{u}_l^{\mathrm{H}}\mathbf{H}_{\mathrm{SI}}$.

To efficiently solve $(\mathcal{P}5)$, we utilize MO. By normalizing the power constraint (10b), we introduce a modified matrix $\mathbf{V}$, composing columns $\{\mathbf{v}_1, \ldots, \mathbf{v}_{K+1}\}$, such that $\mathrm{Tr}(\mathbf{V}\mathbf{V}^{\mathrm{H}}) = \mathrm{Tr}(\mathbf{W}\mathbf{W}^{\mathrm{H}}) + ||\mathbf{z}||_2^2 = 1$, where $\mathbf{v}_k = [\mathbf{w}_k^{\mathrm{T}}, z_k]^{\mathrm{T}}$ for $k \in \{1, \ldots, K\}$ and $\mathbf{v}_{K+1} = [\mathbf{s}^{\mathrm{T}}, z_{K+1}]^{\mathrm{T}}$. Moreover, $\mathbf{z} = [z_1, \ldots, z_{K+1}]$ is an auxiliary vector introduced to simplify power normalization while preserving the constraint. This normalization leads to a complex sphere manifold as $\mathcal{M} = \{\mathbf{V} \in \mathbb{C}^{(M+1)\times(K+1)} \,|\, \mathrm{Tr}(\mathbf{V}\mathbf{V}^{\mathrm{H}}) = 1\}$. Thereby, $(\mathcal{P}5)$ is transformed into an unconstrained optimization problem on $\mathcal{M}$ and given by

$$(\mathcal{P}6): \min_{\mathbf{V}\in\mathcal{M}} \quad f(\mathbf{V}), \tag{17}$$

where $f(\mathbf{V})$ is defined in (18), in which $\hat{\mathbf{h}}_k = \sqrt{p_{\max}}[\mathbf{h}_k, 0]$, $\hat{\mathbf{g}}_{lj} = \sqrt{p_{\max}}[\mathbf{g}_{lj}, 0]$, and $\hat{\mathbf{g}}_{\mathrm{SI},l} = \sqrt{p_{\max}}[\mathbf{g}_{\mathrm{SI},l}, 0]$ are adjusted to match the problem's dimensionality and scaling. Here, the optimization variable $\mathbf{V}$ is constrained to lie on $\mathcal{M}$, aligning with the MO framework. To optimize (17) on $\mathcal{M}$, the MO-based beamforming algorithm, outlined in **Algorithm 1**, involves the following key steps [14], [15]:

Gradient Computation: Compute the Riemannian gradient of $f(\mathbf{V})$ on $\mathcal{M}$. This is achieved by projecting the Euclidean gradient onto the tangent space $T_{\mathbf{V}_t}\mathcal{M}$ at the current point $\mathbf{V}_t$. The Euclidean gradient of $f(\mathbf{V})$, i.e., $\nabla_{\mathbf{V}_t} f(\mathbf{V})$, is given by (19), where

$$B_l \triangleq \sum\nolimits_{j=1}^{L}|\beta_j|^2\Big|\hat{\mathbf{g}}_{lj}^{\mathrm{H}}\Big(\sum\nolimits_{q=1}^{K+1}\mathbf{V}\mathbf{E}_q\Big)\Big|^2 + \beta_{\mathrm{SI}}\Big|\hat{\mathbf{g}}_{\mathrm{SI},l}^{\mathrm{H}}\Big(\sum\nolimits_{q=1}^{K+1}\mathbf{V}\mathbf{E}_q\Big)\Big|^2 + \sigma^2,$$

$$D_l \triangleq \sum\nolimits_{n=1}^{L}|\beta_n|^2\hat{\mathbf{g}}_{ln}^{\mathrm{H}}\Big(\sum\nolimits_{q=1}^{K+1}\mathbf{V}\mathbf{E}_q\Big)\hat{\mathbf{g}}_{ln}\Big(\sum\nolimits_{q=1}^{K+1}\mathbf{E}_q^{\mathrm{H}}\Big) + \beta_{\mathrm{SI}}\hat{\mathbf{g}}_{\mathrm{SI},l}^{\mathrm{H}}\Big(\sum\nolimits_{q=1}^{K+1}\mathbf{V}\mathbf{E}_q\Big)\hat{\mathbf{g}}_{\mathrm{SI},l}\Big(\sum\nolimits_{q=1}^{K+1}\mathbf{E}_q^{\mathrm{H}}\Big).$$

Search Direction: Determine the search direction by choosing a descent direction in $T_{\mathbf{V}_t}\mathcal{M}$, and is given by $\boldsymbol{\eta}_{t+1} = -\mathrm{grad}_{\mathbf{V}_{t+1}} f(\mathbf{V}) + \nu_t \mathcal{T}_{\mathbf{V}_t\to\mathbf{V}_{t+1}}(\boldsymbol{\eta}_t)$, where $\boldsymbol{\eta}_t$ is the current search direction and ν_t is computed using the Hestenes-Stiefel approach.

Retraction (Mapping): Apply a retraction operation, $R_{\mathbf{V}_t}(\alpha_t\eta_t) = \mathrm{unt}(\alpha_t\eta_t)$, where α_t denotes the step size, to map the updated point, which lies in the tangent space, back onto $\mathcal{M}$. This ensures that the next iterate remains on the manifold after the update. Interested readers are referred to [14], [15] and related literature for more insights and algorithmic details.

VI. Simulation Results

Simulation examples are provided to evaluate all three protocols in terms of C&S. The 3GPP UMi model is used for the large-scale fading ζ_i with f_c operating frequency [16, Table B.1.2.1]. The BS is placed at the origin. Users are randomly distributed within circular regions centered around the BS, with an inner radius of $50\,\mathrm{m}$ and an outer radius of $70\,\mathrm{m}$. Targets are distributed within circular regions centered at the BS, with an inner radius of $20\,\mathrm{m}$ and an outer radius of $30\,\mathrm{m}$. The simulation consists of 10^3 Monte Carlo trials. Unless otherwise specified, the simulation parameters are provided in Table I.

Fig. 3 investigates the communication sum rate (i.e., left y-axis) and sensing sum rate (i.e., right y-axis) as functions of the number of BS antennas for all three transmission protocols. A higher number of BS antennas leads to an increase in both C&S sum rates across all protocols, effectively leveraging the

$$f(\mathbf{W}) = \sum_{k=1}^{K} \frac{\hat{\mu}_k |\mathbf{h}_k^{\mathrm{H}} \mathbf{W} \mathbf{E}_k|^2}{\sum_{i=1}^{K+1} |\mathbf{h}_k^{\mathrm{H}} \mathbf{W} \mathbf{E}_i|^2 + \sigma^2} + \sum_{l=1}^{L} \frac{\hat{\mu}_{K+l} |\beta_l|^2 \left| \mathbf{g}_{ll}^{\mathrm{H}} \left(\sum_{q=1}^{K+1} \mathbf{W} \mathbf{E}_q \right) \right|^2}{\sum_{j=1}^{L} |\beta_j|^2 \left| \mathbf{g}_{lj}^{\mathrm{H}} \left(\sum_{q=1}^{K+1} \mathbf{W} \mathbf{E}_q \right) \right|^2 + \beta_{\mathrm{SI}} \left| \mathbf{g}_{\mathrm{SI},l}^{\mathrm{H}} \left(\sum_{q=1}^{K+1} \mathbf{W} \mathbf{E}_q \right) \right|^2 + \sigma^2} \tag{16}$$

$$f(\mathbf{V}) = -\sum_{k=1}^{K} \frac{\hat{\mu}_k |\hat{\mathbf{h}}_k^{\mathrm{H}} \mathbf{V} \mathbf{E}_k|^2}{\sum_{i=1}^{K+1} |\hat{\mathbf{h}}_k^{\mathrm{H}} \mathbf{V} \mathbf{E}_i|^2 + \sigma^2} - \sum_{l=1}^{L} \frac{\hat{\mu}_{K+l} |\beta_l|^2 \left| \hat{\mathbf{g}}_{ll}^{\mathrm{H}} \left(\sum_{q=1}^{K+1} \mathbf{V} \mathbf{E}_q \right) \right|^2}{\sum_{j=1}^{L} |\beta_j|^2 \left| \hat{\mathbf{g}}_{lj}^{\mathrm{H}} \left(\sum_{q=1}^{K+1} \mathbf{V} \mathbf{E}_q \right) \right|^2 + \beta_{\mathrm{SI}} \left| \hat{\mathbf{g}}_{\mathrm{SI},l}^{\mathrm{H}} \left(\sum_{q=1}^{K+1} \mathbf{V} \mathbf{E}_q \right) \right|^2 + \sigma^2} \tag{18}$$

$$\begin{aligned} \nabla_{\mathbf{V}_t} f(\mathbf{V}) = \sum\nolimits_{k=1}^{K} -\hat{\mu}_k \left(\frac{2 \hat{\mathbf{h}}_k^{\mathrm{H}} \mathbf{V}_t \mathbf{E}_k \hat{\mathbf{h}}_k \mathbf{E}_k^{\mathrm{H}}}{\sum_{j=1}^{K+1} |\hat{\mathbf{h}}_k^{\mathrm{H}} \mathbf{V}_t \mathbf{E}_j|^2 + \sigma^2} - \sum_{i=1}^{K+1} \frac{2 |\hat{\mathbf{h}}_k^{\mathrm{H}} \mathbf{V}_t \mathbf{E}_k|^2 \hat{\mathbf{h}}_k^{\mathrm{H}} \mathbf{V}_t \mathbf{E}_i \hat{\mathbf{h}}_k \mathbf{E}_i^{\mathrm{H}}}{\left(\sum_{j=1}^{K+1} |\hat{\mathbf{h}}_k^{\mathrm{H}} \mathbf{V}_t \mathbf{E}_j|^2 + \sigma^2 \right)^2} \right) \\ - \sum\nolimits_{l=1}^{L} \hat{\mu}_{K+l} |\beta_l|^2 \left(\frac{2}{B_l} \hat{\mathbf{g}}_{ll}^{\mathrm{H}} \left(\sum\nolimits_{q=1}^{K+1} \mathbf{V} \mathbf{E}_q \right) \hat{\mathbf{g}}_{ll} \left(\sum\nolimits_{q=1}^{K+1} \mathbf{E}_q^{\mathrm{H}} \right) - \frac{2}{B_l^2} \left| \hat{\mathbf{g}}_{ll}^{\mathrm{H}} \left(\sum\nolimits_{q=1}^{K+1} \mathbf{V} \mathbf{E}_q \right) \right|^2 D_l \right) \end{aligned} \tag{19}$$

Algorithm 1 : Beamforming Algorithm

Initialization: Initial point $\mathbf{V}_0 \in \mathcal{M}$, reduction factor $\theta_\rho > 1$, a minimum acceptable distance $d_{\min}$, the convergence tolerance $\delta_1 > 0$ and $\delta_2 > 0$, and set $t_1 = 0$.
while $\mathrm{dist}(f(\mathbf{V}_{t_1}), f(\mathbf{V}_{t_1+1})) \geq \delta_2$ **do**
  Update $\boldsymbol{\eta}_0 = -\mathrm{grad}_{\mathbf{V}_0} f(\mathbf{V})$ and set $t = 0$.
  while $\|\mathrm{grad}_{\mathbf{V}_t} f(\mathbf{V})\|_2 > \delta_1$ **do**
    Calculate Armijo backtracking line search step α_t.
    Update $\mathbf{V}_{t+1}$ using the retraction $R_{\mathbf{V}_t}(\alpha_t \boldsymbol{\eta}_t)$.
    Update $\mathcal{T}_{\mathbf{V}_t \to \mathbf{V}_{t+1}}(\boldsymbol{\eta}_t)$.
    Compute the Hestenes-Stiefel parameter ν_t.
    Update the search direction $\boldsymbol{\eta}_{t+1}$.
    $t \leftarrow t + 1$.
  end while
  if $t = 0$ **then**
    $\rho_{t+1} = \rho_t$.
  else
    $\rho_{t+1} = \theta_\rho \rho_t$.
  end if
  $t_1 \leftarrow t_1 + 1$.
  $\mathbf{V}_0 \leftarrow \mathbf{V}_{t+1}$.
end while
Output: $\mathbf{W}^* = \mathbf{V}^*(1 : M, K + 1)$.

TABLE I: Simulation settings.

Parameter	Value	Parameter	Value
f_c	3 GHz	$\lvert\beta_l\rvert$	8×10^{-4}
σ^2	-80 dBm	$\{M, N\}$	16
τ_c	200	K	4
$\{\tau_s, \tau_u\}$	$\tau_c/2$	L	2
$\{\tau_1, \tau_2, \tau_3\}$	$\tau_c/3$	$p_{\max}$	30 dBm
β_{SI}	-70 dB	K_{SI}	3 dB

spatial multiplexing advantages of a larger antenna array. Fig. 3 shows that TP_1 protocol outperforms both TP_2 and TP_3. This advantage is primarily due to its use of the entire coherence interval for both C&S tasks. Although TP_2 eliminates interference between C&S functions, its limited time allocation for both tasks results in the lowest C&S rate performance.

Nevertheless, when evaluating these protocols, it is essential to consider the achieved rates and the ability to locate targets accurately. To this end, Fig. 4 compares the beampattern gains. In particular, the BS transmit signal, $\mathbf{x}$, represents the outward-projected energy intended to illuminate the targets. The received combiners are designed to capture the reflected signals, focusing on target echoes. The three key beampatterns are defined as

$$p_1(\theta) = \left| \mathbf{a}_t^{\mathrm{H}}(\theta_l) \mathbf{x}^* \right|^2, \tag{20a}$$

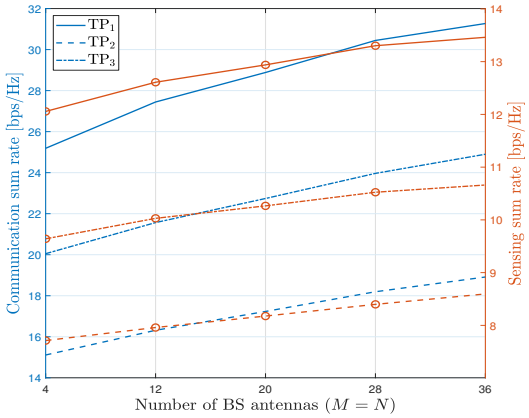

Fig. 3: C&S sum rate versus the number of BS antennas.

$$p_2(\theta) = \left| (\mathbf{u}_l^*)^{\mathrm{H}} \mathbf{a}_r(\theta_l) \right|^2, \tag{20b}$$

$$p_3(\theta) = \left| (\mathbf{u}_l^*)^{\mathrm{H}} \mathbf{A}(\theta_l) \mathbf{x}^* \right|^2, \tag{20c}$$

where (20a) describes how the transmitted energy spreads as a function of angle θ, while (20b) characterizes the system's sensitivity to incoming signals across different angles during reception. Finally, (20c) offers a combined representation, integrating the effects of both transmission and reflection processing.

It is interesting that while the transmit beam gains for TP_1 and TP_3 (the first sub-figures in Fig. 4a and Fig. 4c, respectively) struggle in accurately locating the targets, mainly target two, the transmit beam gain for TP_2 (the first sub-figure in Fig. 4b) exhibits a significantly improved ability to locate all the targets. This is due to the absence of communication interference in the TP_2, which utilizes scheduled transmissions in two separate time slots. Conversely, with all three protocols, the targets can be located through receive and combined beampattern gains, with TP_2 providing the highest gains.

Fig. 5 illustrates the effect of the number of users on communication (i.e., left y-axis) and sensing (i.e., right y-axis) performance. In particular, it serves as a measure of inter-system interference, i.e., communication-sensing interference. In TP_1 and TP_3, the communication rate improves as the number of users increases, whereas the sensing rate declines. This is due to their simultaneous operation of C&S. Thus, as the number of users grows, communication interference on sensing becomes more severe. Also, more resources are allocated to communication due to higher demand, resulting in a decrease

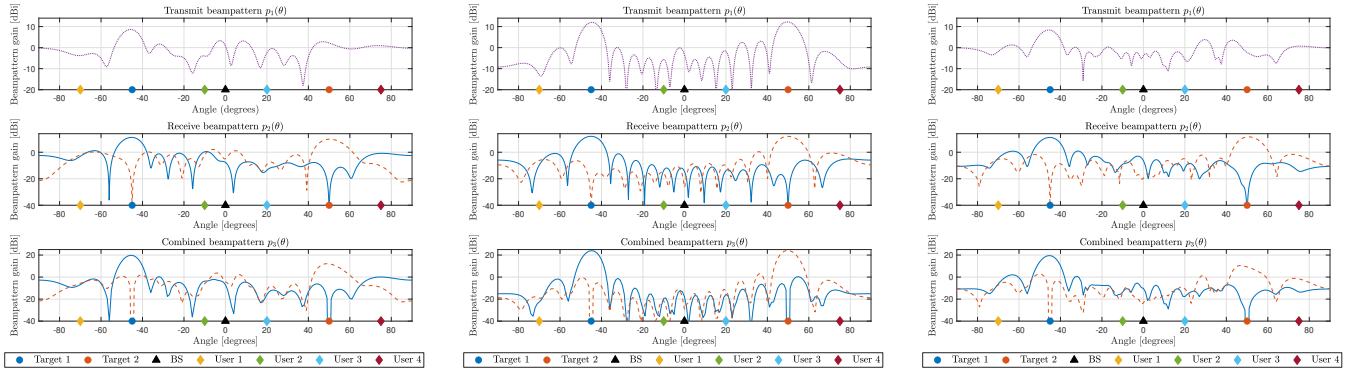

(a) TP_1 protocol. **(b)** TP_2 protocol. **(c)** TP_3 protocol.

Fig. 4: The beampattern gains all three protocols.

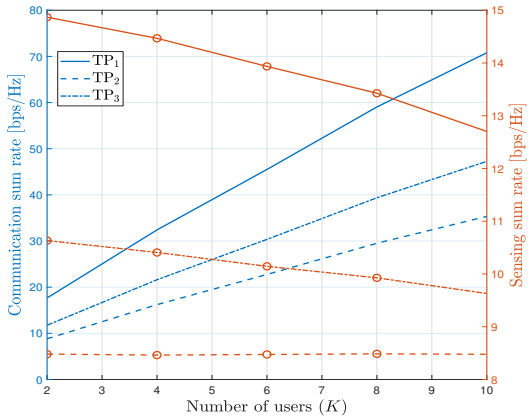

Fig. 5: C&S sum rate versus the number of users.

in sensing performance. However, TP_3 experiences a slightly lower sensing rate reduction compared to TP_1, as simultaneous C&S occur only during a portion of the coherence interval, i.e., τ_2. Conversely, due to the separate C&S functions, in TP_2, C&S do not interfere with each other.

VII. Conclusion

In ISAC, C&S tasks can be scheduled concurrently, sequentially, or as a hybrid of both modalities. Surprisingly, the literature has focused exclusively on concurrent scheduling. This work has thus compared these three modes in detail and uncovered several insights. When employing the TP_1 and TP_3 protocols in ISAC systems, utilizing a sensing metric that considers both transmit and receiver beam gains is essential. Standard metrics, such as transmit beampattern gain or MSE of the transmit beampattern, may be insufficient for these protocols. In contrast, while TP_2 can be easily implemented using simple sensing metrics (e.g., transmit beampattern gain) with eliminated communication-sensing interference, it is unsuitable for applications requiring high communication performance.

Selecting an ISAC transmission protocol to implement both C&S functions depends on the requirements of the application scenario and the hardware capabilities and complexity of the system. Data rate (for both C&S) and target location accuracy are crucial factors in determining the most effective protocol. Also, incorporating advanced technologies, such as adaptive beamforming and resource allocation, must be consistent with the performance criteria needed for each function.

References

[1] F. Liu *et al.*, "Integrated sensing and communications: Toward dual-functional wireless networks for 6G and beyond," *IEEE J. Sel. Areas Commun.*, vol. 40, no. 6, pp. 1728–1767, Jun. 2022.

[2] A. Hakimi, D. Galappaththige, and C. Tellambura, "A roadmap for NF-ISAC in 6G: A comprehensive overview and tutorial," *Entropy*, vol. 26, no. 9, Sept. 2024.

[3] Z. Xiao and Y. Zeng, "Waveform design and performance analysis for full-duplex integrated sensing and communication," *IEEE J. Sel. Areas Commun.*, vol. 40, no. 6, pp. 1823–1837, Jun. 2022.

[4] Z. Liu, S. Aditya, H. Li, and B. Clerckx, "Joint transmit and receive beamforming design in full-duplex integrated sensing and communications," *IEEE J. Sel. Areas Commun.*, vol. 41, no. 9, pp. 2907–2919, Sept. 2023.

[5] Z. He *et al.*, "Full-duplex communication for ISAC: Joint beamforming and power optimization," *IEEE J. Sel. Areas Commun.*, vol. 41, no. 9, pp. 2920–2936, Sept. 2023.

[6] M. Mohammadi, Z. Mobini, D. Galappaththige, and C. Tellambura, "A comprehensive survey on full-duplex communication: Current solutions, future trends, and open issues," *IEEE Commun. Surveys Tuts.*, vol. 25, no. 4, pp. 2190–2244, 4th Quart. 2023.

[7] F. Liu, Y.-F. Liu, A. Li, C. Masouros, and Y. C. Eldar, "Cramér-Rao bound optimization for joint radar-communication beamforming," *IEEE Trans. Signal Process.*, vol. 70, pp. 240–253, Jan. 2022.

[8] M. A. Richards, J. A. Scheer, and W. A. Holm, Eds., *Principles of Modern Radar: Basic principles*, ser. Radar, Sonar and Navigation. Institution of Engineering and Technology, 2010.

[9] P. Stoica, J. Li, and Y. Xie, "On probing signal design for MIMO radar," *IEEE Trans. Signal Process.*, vol. 55, no. 8, pp. 4151–4161, Jul. 2007.

[10] G. Cui, H. Li, and M. Rangaswamy, "MIMO radar waveform design with constant modulus and similarity constraints," *IEEE Trans. Signal Process.*, vol. 62, no. 2, pp. 343–353, Jan. 2014.

[11] J. C. Bezdek and R. J. Hathaway, "Convergence of alternating optimization," *Neural, Parallel & Scientific Computations*, vol. 11, no. 4, pp. 351–368, Dec. 2003.

[12] S. Stanczak, *Fundamentals of Resource Allocation in Wireless Networks Theory and Algorithms*, 2nd ed. Berlin, Heidelberg: Springer Berlin Heidelberg, 2008.

[13] K. Shen and W. Yu, "Fractional programming for communication systems—part I: Power control and beamforming," *IEEE Trans. Signal Process.*, vol. 66, no. 10, pp. 2616–2630, May 2018.

[14] C. Liu and N. Boumal, "Simple algorithms for optimization on Riemannian manifolds with constraints," *Appl. Math. Optim.*, vol. 82, pp. 949–981, Mar. 2020.

[15] S. Zargari, D. Galappaththige, C. Tellambura, and H. Vincent Poor, "A Riemannian manifold approach to constrained resource allocation in ISAC," *IEEE Trans. Commun.*, pp. 1–1, 2024.

[16] "3GPP TR 36.814, further advancements for E-UTRA physical layer aspects, V.9.0.0 Rel. 9," Mar. 2010. Available Online: https://portal.3gpp.org/desktopmodules/Specifications/SpecificationDetails.aspx?specificationId=2493.